The Power Stroke Driven by ATP Binding in CFTR As Studied by Molecular Dynamics Simulations

Tomoka Furukawa-Hagiya,[†] Tadaomi Furuta,[†] Shuntaro Chiba,[†] Yoshiro Sohma,[‡] and Minoru Sakurai*[,†]

[†]Center for Biological Resources and Informatics, Tokyo Institute of Technology, 4259-B-62, Nagatsuta-cho, Midori-ku, Yokohama, 226-8501, Japan

[‡]Department of Pharmacology, Keio University School of Medicine, Shinjuku, Tokyo 160-8582, Japan

Ⓢ *Supporting Information*

ABSTRACT: Cystic fibrosis transmembrane conductance regulator (CFTR) is a chloride channel belonging to the ATP binding cassette (ABC) protein superfamily. Currently, it remains unclear how ATP binding causes the opening of the channel gate at the molecular level. To clarify this mechanism, we first constructed an atomic model of the inward-facing CFTR using the X-ray structures of other ABC proteins. Molecular dynamics (MD) simulations were then performed to explore the structure and dynamics of the inward-facing CFTR in a membrane environment. In the MgATP-bound state, two nucleotide-binding domains (NBDs) formed a head-to-tail type of dimer, in which the ATP molecules were sandwiched between the Walker A and signature motifs. Alternatively, one of the final MD structures in the apo state was similar to that of a "closed-apo" conformation found in the X-ray analysis of ATP-free MsbA. Principal component analysis for the MD trajectory indicated that NBD dimerization causes significant structural and dynamical changes in the transmembrane domains (TMDs), which is likely indicative of the formation of a chloride ion access path. This study suggests that the free energy gain from ATP binding acts as a driving force not only for NBD dimerization but also for NBD−TMD concerted motions.
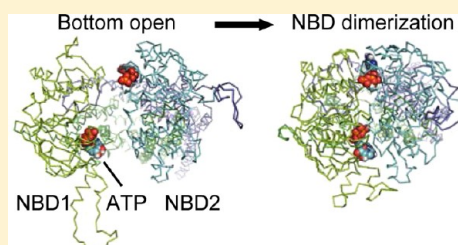
INTRODUCTION

Cystic fibrosis (CF) is a common autosomal recessive disorder usually found in populations of white Caucasians and is caused by mutations in the gene for the CFTR chloride channel.[1,2] CFTR is a member of the ABC protein superfamily (ABCC7).[3] Similar to other ABC proteins, CFTR consists of two nucleotide-binding domains (NBD1 and NBD2) and two transmembrane domains (TMD1 and TMD2), and each TMD has six transmembrane helices (TMs) connected by intra- and extracellular loops (ICLs and ECLs, respectively). Although the TMDs show little sequence homology, the NBDs of all ABC proteins have extensive amino acid sequence identity with several conserved motifs (described below).[4,5] In particular, CFTR has a unique domain called the "regulatory domain" (RD) that keeps the channel closed unless it is phosphorylated by PKA.[6] Once the RD is phosphorylated, the two NBDs are thought to approach each other closely.[7]

Electrophysiological studies of CFTR channel gating revealed that the NBDs dimerize in a head-to-tail fashion, as has been observed with other ABC proteins.[8−10] Structural studies have shown that two ATP molecules are buried in two composite interfacial sites,[11] which are called the ATP-binding pockets (ABP1 and ABP2). ABP2 is a "canonical" ATP-binding pocket and includes the following seven common motifs (shown in Supporting Information Figure S1): the Walker A and B motifs,[12] A-loop,[13] Q-loop,[14] and H-loop[5,15] on the NBD2 side and the signature motif (C-loop)[16] and D-loop[17,18] on the NBD1 side. ABP1 is a "noncanonical" ATP-binding pocket and

lacks the catalytic glutamate of Walker B (Glu → Ser573), and some catalytically important residues are noncanonical: His → Ser605 (of the H-loop), Gly → His1348 and Gln → His1350 (of the signature motif). ABP1 has a higher ATP binding affinity than ABP2, which is likely due to the differences in their primary structures.[10,19,20] The features of CFTR's two ABPs distinguish CFTR from the other members of the ABC superfamily.

As a result of the NBD dimerization, the CFTR protein is thought to undergo a large structural change from inward- to outward-facing conformations, eventually leading to the opening of the channel. Zhou et al.[21] proposed that the two ABPs play the following different roles in CFTR gating: the hydrolysis of ATP at ABP2 leads to dimer dissociation and the closing of the channel, whereas ATP binding to ABP1 may contribute to the stabilization of the open channel conformation.[22] These phenomenological findings should be confirmed using atomic-level 3D structural information to elucidate the functional mechanism of CFTR in more detail.

The structure of full-length human CFTR has not been determined, although the crystal structures of CFTR NBD1 and NBD2 have been published.[23,24] Instead, several homology models based on the X-ray structures of the microbial ABC transporters Sav1866 and MsbA have been published, providing

invaluable insight into the specific structural features of CFTR.[25−30] Despite the significant contributions of these structural studies to our understanding of the CFTR gating mechanism, they can provide only static snapshots of the transport cycle. Therefore, time-resolved techniques have been employed to gain insight into the dynamic properties of CFTR. Recently, molecular dynamics (MD) simulation studies of the full-length CFTR, combined with cysteine scanning and patch clamp experiments, successfully provided atomic-level information about the architecture of the anion conduction path and the location of a "bottleneck" in the pore.[29] These MD simulations were performed using initial structures based on the crystal structure of Sav1866 and, hence, provided specific structural features for the outward-facing conformation (open channel conformation) of CFTR. In particular, these studies focused on the structural details of TMDs (or the pore geometry) because they might be directly related to the anion conduction; however, these studies did not provide sufficient information about the structure of the NBD region and NBD−TMD interface/coupling. Currently, the atomic details of the inward-facing conformation (closed channel) and its transition to an outward-facing conformation (channel opening) of CFTR remains unclear, although such information is indispensable for comprehensively understanding the gating cycle of CFTR.

In this study, we focus on the mechanisms driving the power stroke of the protein from inward- to outward-facing conformations in conjunction with ATP binding. For this purpose, we first performed homology modeling for the inward-facing conformation of CFTR and subsequently conducted MD simulations, starting from the resulting structures. It was found that binding of ATP and Mg^{2+} causes the dimerization of two NBDs in a head-to-tail fashion, whereas in the apo state, the NBDs converged to a semiopen conformation similar to the "closed-apo" conformation of MsbA.[31] Detailed analyses of the hydrogen bond network around the bound ATP molecules and of the time course of dimerization demonstrated that the ATP molecules act as "molecular glue" to make contact between the NBDs. Additionally, we show that NBD dimerization causes the collective motion of the whole protein to activate the motion of the TMDs and creates an access path for chloride ions from the intracellular medium to the protein interior. Finally, we discuss the mechanism of NBD dimerization in light of recent experimental results for other full-length ABC transporters.

■ METHODS

Homology Modeling. The flowchart of homology modeling performed in this study is depicted in Supporting Information Figure S2. The amino acid sequence of human CFTR was obtained from the UniProt database (accession no. P13569). This protein has 1480 residues and consists of two TMDs, two NBDs, and one RD, which are arranged in the following order: TMD1-NBD1-RD-TMD2-NBD2. A sequence search failed to identify a homologue of known structure with significant similarity to the entire CFTR sequence. Therefore, the present sequence alignment was performed using a "hybrid" template that was obtained by joining together available experimental structures for the NBDs and TMDs. The following structural templates for the modeling of NBD1 and NBD2 were found by PSI-BLAST search:[32] the human f508a NBD1 domain complexed with ATP and Mg^{2+} (PDB code: 1XMI)[24] for NBD1 (residues 389−645) and the human NBD2 complexed with n6-phenylethyl-ATP (P-ATP) (PDB code:

3GD7) for NBD2 (residues 1202−1427), where P-ATP was replaced by ATP and Mg^{2+} in reference to the NBD1 template. For the TMDs, a crystallographic structure of a mouse P-glycoprotein transporter (P-gp, ABCB1; PDB code 3G5U)[33] was used as a template because this protein has an N-glycosylation site on ECL1 (TMD1) similar to that present on ECL4 (TMD2) of CFTR. We performed sequence alignments between each domain of CFTR and the corresponding template using the Clustal W2 program.[34] Portions of the α-helices and the intracellular loops (ICLs) were aligned according to the previous reports.[26,27,35] This alignment was subsequently refined using constraints derived from TMDs and ICLs.

Unlike the other ABC transporters, CFTR has a looplike structure called the "regulatory insertion (RI)" (residues 415−432) in NBD1 located between strands β1 and β2 of the ABC-specific β subdomain. In the crystal structure of NBD1, this loop region was disordered and thereby constructed in the step of 3D modeling described below (the disordered "linker insertion" region (residues 1185−1201) in NBD2 was also modeled). However, the homology modeling was not applied for RD (residues 638−843) because the split channels with no RD were highly active without phosphorylation.[36] The N-terminal (residues 1−56) and C-terminal (residues 1428−1480) regions were also not considered in this study because no appropriate templates have been found.

3D homology modeling was performed using Modeler 9v8 based on the sequence alignments.[37] Then, we adopted the "automodel" protocol[37] with no special restraints imposed on the protein structure. We first created 10 models and selected the best structure with the following criterion: the lowest DOPE (discreted optimized protein energy)[38] and the highest GA341 scores.[39] These scores are usually employed to rank the models on the basis of their energy levels. We confirmed that the α-helix bundle in the TMD region in the same way as that of the template, and their stereochemical quality of the resulting model was validated with PROCHECK.[40] Furthermore, the model was assessed by comparison with various experimental information about the pore-forming residues of CFTR.[29,41−52]

Molecular Dynamics Simulation. The CFTR model structure obtained above was inserted into the optimal position of a 1-palmitoyl-2-oleylphosphatidylcholine (POPC) lipid bilayer based on the hydrophobicity of the protein residues and the transmembrane region of the template structure (P-gp) with reference to the OPM (Orientations of Proteins in Membranes) database.[53] The bilayer structure used here was prepared by quadruplicating a bilayer consisting of 128 POPC molecules downloaded from Tieleman's Web site (available for download from http://moose.bio.ucalgary.ca/), then the lipid molecules were fit to TMDs using the "shrinking" method developed by Kandt et al.;[54] consequently, 484 POPC molecules were present in the bilayer, where the shrinking cycles were performed with the InflateGRO script.[54] Subsequently, this system (protein and membrane) was solvated by water molecules, where water molecules inside the bilayer (hydrophobic region) were removed by visual inspection, and Na^+ and Cl^- ions were inserted randomly into the solvent to preserve the electric neutrality in both the MgATP-bound and apo states. The resultant system in the MgATP-bound state has 69 001 water molecules, 2 Na^+, and 18 Cl^- ions; and the resultant system in the apo state has 69 061 water molecules, 2 Na^+, and 22 Cl^- ions. The total number of atoms in the
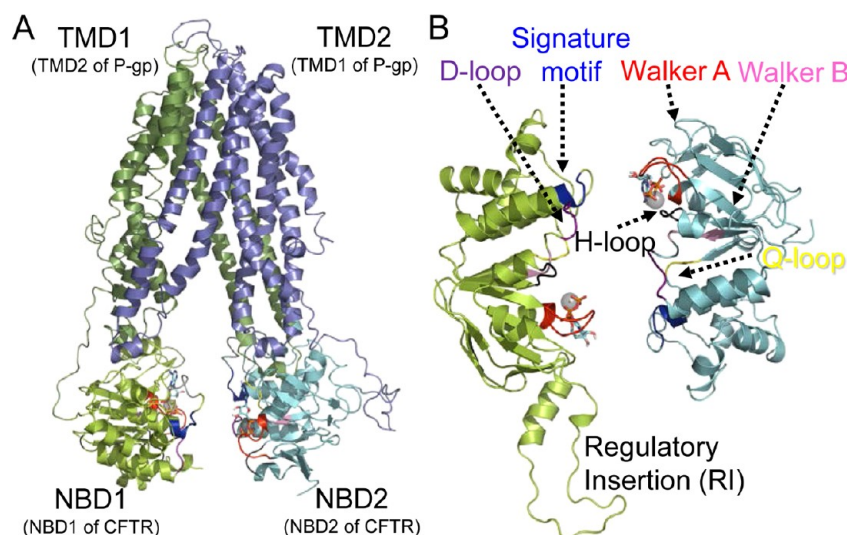
Figure 1. Homology model of human CFTR in the inward-facing conformation. (A) The full-length homology model of CFTR. The TMD1, NBD1, TMD2, and NBD2 are colored in green, lime, blue, and cyan, respectively, with ribbon representation. ATP molecules and Mg^{2+} ions are represented by sticks (white for hydrogen, cyan for carbon, blue for nitrogen, red for oxygen, and orange for phosphorus) and spheres (gray). (B) Enlarged view from the bottom. The conserved sequence motifs are colored in red (Walker A), pink (Walker B), yellow (Q-loop), blue (signature motif), purple (D-loop), and black (H-loop).

MgATP-bound and apo states was 244 304 and 244 281, respectively.

Each system was relaxed by the steepest descent minimization until the maximum force on any atom became less than 100 kJ/(mol Å). The MD simulation was carried out according to the following protocol: the systems were first equilibrated for 40 ns with harmonic restraints on all the heavy atoms of proteins (as well as ATP and Mg^{2+} ions in the MgATP-bound state) with the strength of 10 kJ/(mol Å^2), by which the lipids were packed appropriately around the protein; then the production runs were carried out for a total of 100 ns without all restraints. To reduce the sampling problems in protein simulations, in addition, we performed three 20-ns-long MD simulations for each system in the study, in a total of six simulations. All replicates were initiated with different sets of random velocities. All simulations were conducted under the NPT conditions with the Nosé−Hoover thermostat[55,56] and Parrinello−Rahman barostat.[57] The temperature of the system was kept at 310 K, with separate coupling of solutes (e.g., protein, nucleotides, and lipids) and solvents. The pressure was kept to 1 bar. During the MD simulations, the covalent bonds were constrained by the LINCS algorithm,[58,59] and SPC water molecules[60] were constrained with the SETTLE algorithm.[61] The van der Waals interactions were used with a cutoff distance of 12 Å. The electrostatic interactions were calculated using the particle-mesh Ewald method[62,63] with a real space cutoff of 12 Å.

All the MD simulations were performed using the GROMACS v4.0.7. package.[64] The GROMOS-87 force field[65−67] was used for the protein, and the SPC model was used for the water molecules. In particular, the H-loop motif (His1402) was doubly protonated in the MgATP-bound state and singly protonated in the apo state. The force field for ATP with a net charge of −4e was obtained by modifying the original GROMACS force field; we removed the hydrogen atom from the protonated γ-phosphate and redistributed the partial charges evenly over the phosphate oxygen atoms. As for the

POPC molecules, we used the topology developed by Berger et al.[68] and later modified by Tieleman and Berendsen.[69]

For analyzing MD trajectories, the root-mean-square deviation (rmsd) and several intermotif and interresidue distances were calculated using GROMACS tools. 3D graphics were produced using Pymol (http://www.pymol.org). To identify the most prominent characteristics of the motions along a simulation trajectory, a principal component analysis (PCA)[70,71] was carried out by using GROMACS tools, and the eigenvectors of PCs were visualized with the aid of VMD.[72]

■ **RESULTS**

3D Structural Model of CFTR. As the first step of homology modeling, we performed a sequence alignment (see the Methods section). The structures of CFTR NBD1 and NBD2 have been modeled using the crystal structures of human CFTR NBD1 (PDB code: 1XMI)[24] and human CFTR NBD2 (PDB code: 3GD7) as templates. The results of the sequence alignments for the NBDs are shown in Supporting Information Figure S3A and B, where the sequence identities of NBD1 and NBD2 had 98% and 96% homology, respectively, to the corresponding templates. The homology modeling of TMDs required additional information because there was relatively low sequence similarity in the TMD regions. The biochemical study showed that N-glycosylation occurs in the ECL4 connecting TM7 with TM8 in CFTR[73] as well as in the ECL1 connecting TM1 with TM2 in the template protein (P-gp).[74] These data imply that from a biochemical viewpoint, TMD2 of CFTR (including ECL4) would be similar to TMD1 of P-gp (including ECL1). Therefore, we aligned TMD2 of CFTR with TMD1 of P-gp, which led to an alignment between TMD1 of CFTR and TMD2 of P-gp. Supporting Information Figure S3C and D shows the results for the alignment between the TMDs of the human CFTR and those of mouse P-gp. A few insertions and deletions were found that occurred as a result of the low identity between the TMDs (TMD1 of CFTR to TMD2 of P-gp, 11.0%; TMD2 of CFTR to TMD1 of P-gp, 13%).

The 3D structure of the whole CFTR protein was modeled using the Modeler program on the basis of the sequence alignments described above. Figure 1 shows the final 3D model of CFTR, which was selected according to the above-mentioned criterion. In accordance with a typical inward-facing structure, this model has an overall tweezers-like structure, such that a large cavity is open to the intracellular side, and the nucleotide binding sites of both NBD1 and NBD2 are exposed to the intracellular space. The quality of this model was evaluated using PROCHECK[40] and was found to be reasonable; the residues were of 83.1% in favored core regions, 15.7% in allowed regions, and relatively low (0.6%) in generously allowed regions and in disallowed regions on the Ramachandran diagram. Furthermore, the homology model of the TMD region of the model was evaluated by comparison with the structural information from the available experimental data, including cysteine-scanning and mutagenesis analysis.[29,41−52] Consequently, it was confirmed that the pore is formed by an internal cavity surrounded by TM1, TM6, and TM12 (Supporting Information Figure S4), which is consistent with the experimental prediction.

Dynamics and Structural Changes. We performed 100 ns MD simulations for both the MgATP-bound and apo states starting from the homology modeling structure shown in Figure 1. As an initial check for the structural stability of the systems and to quantitatively assess the extent of the motions, the $C\alpha$ RMSD of the whole protein from the initial structure was measured using the MD trajectories, and we also calculated the RMSD for each of the following domains: NBD1, NBD2, TMD1, and TMD2 (shown in Figure 2). All of the RMSD
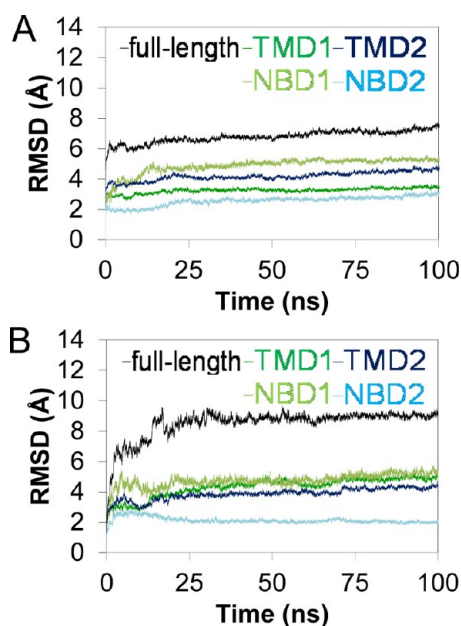

Figure 2. Time dependence of RMSD for the whole protein, TMDs, and NBDs in the MgATP-bound state (A) and in the apo state (B).

values initially increased with time and then reached plateaus after ∼30 ns. In particular, our simulations appeared to be quite stable after 70 ns. The average RMSD value from 70 to 100 ns was calculated for each of the MgATP-bound and apo states; the resulting values for both states were 7.2 and 9.0 Å for the whole protein, 5.3 and 5.1 Å for NBD1, 2.9 and 2.1 Å for NBD2, 3.4 and 4.8 Å for TMD1, and 3.8 and 4.2 Å for TMD2.

Interestingly, the RMSD values of the whole protein and of the TMDs in the apo state exhibited larger fluctuations than those of the MgATP-bound state, whereas those of NBDs were larger in the MgATP-bound state than in the apo state.

Figure 3A and B shows the MD structures in the MgATP-bound and apo states at 100 ns, respectively. Compared with
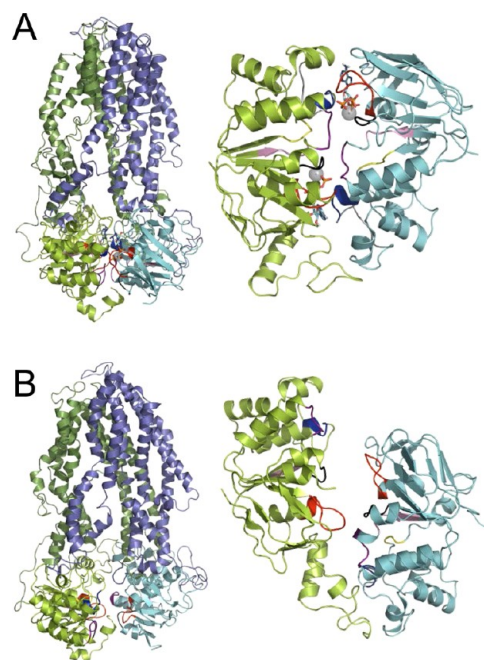

Figure 3. Final MD structures in the MgATP-bound and apo states. Structures of the whole protein (left) and NBDs (right) in the MgATP-bound state (A) and in the apo state (B).

the initial structure (Figure 1), both states appear to undergo significant conformational changes, especially in the NBD regions. In the MgATP-bound state, the two NBDs make direct contact with each other in a head-to-tail fashion as a "canonical" NBD dimer, whereas in the apo state, they make only partial contact. As for the TMDs, the initial structure was well maintained in both the MgATP-bound and apo states.

To clarify the difference of these MD structures, we measured the distance between the Walker A (WA) and signature (C) motifs of each ABP and the distance between the Walker A motif of NBD1 and that of NBD2 spanning the dimer interface (shown in Figure 4). As expected, in the MgATP-bound state, the Walker A motif of one NBD approached the signature motif of the other NBD in both ABPs, hence, forming the canonical ATP sandwich structure. In contrast, in the apo state, the distance between the two Walker A motifs steeply decreased with time and finally reached approximately 5 Å, whereas the Walker A−signature distance remained larger (>10 Å) during the simulation. This result implies that the two Walker A motifs are roughly aligned with one another across the dimer interface; in other words, the two NBDs came close to each other while sliding their positions in the opposite direction along the dimer interface. The final structure is very similar to Mornon's model based on MsbA-closed-apo structure (shown in Supporting Information Figure S6).[27]

Figure 5 shows close-up views of the interface between the two NBDs in the MgATP-bound state. Clearly, ATP molecules are sandwiched between the Walker A motif of one NBD and the signature motif and D-loop of the other NBD in both ABPs
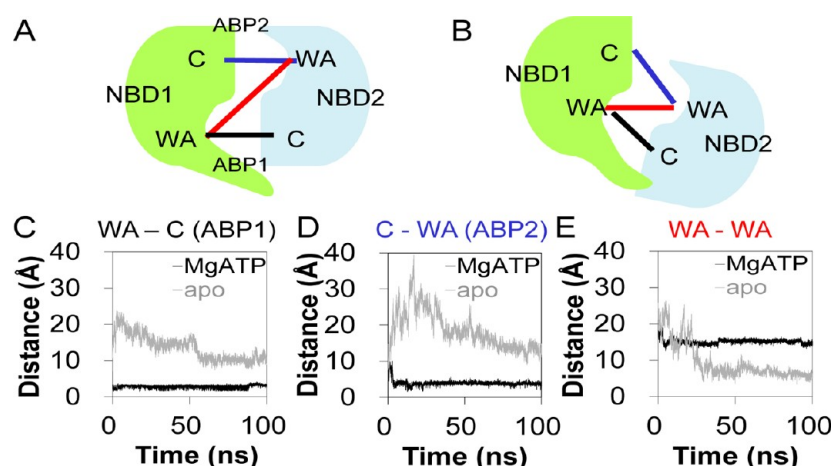
Figure 4. Conformational changes of NBD1 and NBD2 in the MgATP-bound and apo states. Schematic representations of the final NBD conformations in the MgATP-bound state (A) and in the apo state (B), where WA and C stand for Walker A and signature motif, respectively. Time dependence of the minimum distances between WA and C in ABP1 (C) and ABP2 (D) and between WAs (E) in the MgATP-bound state (black) and the apo state (gray).

(shown in Figure 5A). It has been proposed that ATP binding is essential for the formation of the closed NBD dimer, with the two ATP molecules functioning as a molecular "glue".[75,76] Certainly, there were many hydrogen bonds that can be found between the γ-phosphate moieties of the ATP molecules and the neighboring residues of the signature motifs (shown in Figure 5B). In particular, the hydrogen bond formation between an ATP and Gly551 and between the other ATP and His1348 are thought to make important contributions to the stabilization of the NBD dimer. In addition, it is inferred from close inspection of Figure 5 that there may be other factors responsible for the NBD dimerization. In both ABPs, Thr460 (ABP1) and Thr1246 (ABP2) of the Walker A motifs moved toward Asp1377 (ABP1) and Asp579 (ABP2) of the D-loops, respectively, and simultaneously toward the amino acid residues (Gln1352 and Arg555, respectively) located in the downstream regions of the signature motifs. These structural changes should contribute to the strengthening of the contacts between the two NBDs. Therefore, these data suggest that the NBD dimer is stabilized not only by the "glue" effect of ATP but also by the interresidue interactions between the two NBDs.

Time Course of NBD Dimerization in the MgATP-Bound State. To understand the above NBD dimerization process in greater detail, we analyzed the structural changes of the NBD region along the MD trajectory. Several snapshots of the NBD region along the trajectory are shown in Figure 6A–E. Figure 6F shows the distance between the γ-phosphate moieties of the two ATP molecules and their hydrogen bond partners in the signature motifs (see Figure 5B, His1348, and Gly1349 in ABP1, Gly550 and Gly551 in ABP2) and the distance between the ribose sugar/adenine ring of the ATPs and their interaction partners in the helical subdomains of the NBDs (see Figure 5B: Ser1347 in ABP1 and Ile546 in ABP2). Furthermore, to characterize the direct NBD–NBD inter-actions that are not mediated by ATP, we measured the distance between the following residue pairs: Thr460-Asn1377, Thr460-Gln1352, Thr460-His1348, Arg555-Thr1246, Asp579-Thr1246, and Tyr577-His1375 (depicted in Figure 6G).

We found that the closure of ABP1 occurred first, followed by the closure of ABP2 and then NBD dimerization, which was completed in the MgATP-bound state. We then determined the

sequential events occurring at the NBD interface. At 0.5 ns on the ABP1, the distance between the ribose sugar of ATP and Ser1347 had been shortened from 11 Å to 4 Å, and Thr460 of the Walker A motif approached His1348 of the signature motif. At 1.3 ns, a hydrogen bond was formed between Thr460 of Walker A and Asp1377 of the D-loop and, consequently, led to the closure (formation) of ABP1. At 1.6 ns on the ABP2, the distance between His1375 of the D-loop (NBD1) and Tyr577 of the D-loop (NBD2) was shortened, and the two NBDs made direct contact near their central regions (Figure 6G). At 1.8 ns, the adenine ring of ATP, initially attached to the Walker A of NBD2, approached Ile546 of NBD1. Moreover, at 4 ns, the distance between the γ-phosphate of this ATP and the signature motif and the distance between Thr1246 of NBD1 and its interaction partners (Arg555 and Asp579) on NBD2 were significantly shortened; consequently, ABP2 closure occurred. In addition, it was found that in either ABP, the following hydrogen bonds between the Thr residue of the Walker A and the downstream residues of the signature motif were formed: Thr460-Gln1352 in ABP1 and Thr1246-Arg555 in ABP2. It has been confirmed from an electrophysiological study using mutated proteins that the latter hydrogen bonds are essential for the activation of CFTR.[10] After 30 ns, the NBD dimer became stable, as the RMSD of the NBDs reached a plateau at approximately 30 ns (see Figure 2).

It thus appears that a series of structural changes as described above is triggered by the attractive interaction between the ATP and the signature motif at ABP1, which implies that the ATP binding drives the power stroke.[77]

Dynamics of the Intracellular Loops. It has been hypothesized that conformational changes generated by ATP binding and/or hydrolysis are transmitted from the NBDs to the TMDS through noncovalent interactions at the shared interface. According to the X-ray structure of Sav1866, such interactions are generated mainly through the intracellular loops ICL1 and ICL2.[78] This hypothesis is consistent with genetic data showing that the ICL1 of TMD1 interacts with the NBDs.[79] Therefore, it is of great importance to examine the structure of the ICLs. In our homology modeling structure, the ICL1 connecting TM2 and TM3 contacts NBD1, while the ICL2 connecting TM4 and TM5 reaches to the opposite NBD2. Similarly, in the latter half of the protein, the ICL3
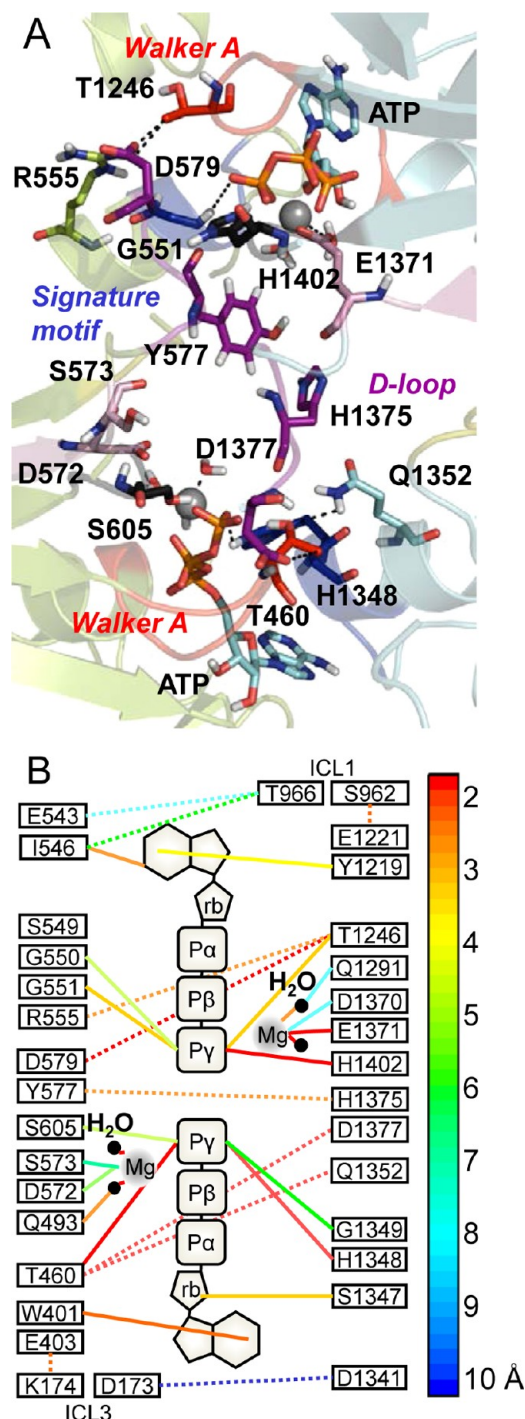
Figure 5. Interactions between ATP/Mg^{2+} and its neighboring residues in the MgATP-bound state. (A) Structure at the ATP-binding pockets in the CFTR-NBD dimer. ATPs, their interacting residues and water molecules are shown by stick representation, with Mg^{2+} shown as a sphere (gray). (B) Schematic diagram of the interaction network around the two ATP molecules bound to the ABPs. The ATP/Mg^{2+}-participated interactions are shown as solid lines, and the direct amino acid−amino acid interactions are shown as dashed lines. The interaction distances are shown in the color gradation from 2.0 (red) to 10.0 (blue) Å.

connecting TM8 and TM9 contacts NBD2, while the ICL4 connecting TM10 and TM11 reaches to the opposite NBD1. Such swappings among the ICLs have been commonly reported for ABC exporters.[28,80] Close inspection of the MD

structure at 100 ns indicated that in the MgATP-bound state, the ICL2-NBD2 contact was formed by interactions between Cys276 and Lys1284 and between Cys276 and Gln1280 (Figures 7A and 7C); similarly, the ICL4-NBD1 contact was formed by interactions between Phe508 and Phe1068 and between Trp496 and Thr1064 (Figures 7B and 7D). These findings are consistent with the results of a previous report by Serohijos et al.[25,28] However, such inter-residue interactions were not observed in the apo state because the secondary structures of ICL4 and the helical domain of NBD1 were disrupted slightly after the simulation (data not shown). Another interesting finding regarding the structure in the MgATP-bound state is that Gln270 of ICL2 approached Lys1292 of the Q-loop in NBD2 (Figure 7A), and Arg1066 of ICL4 was close not only to Ser492 of the Q-loop in NBD1 but also to Mg^{2+} in ABP1 (Figure 7B). The similar structural configurations were found in the NBD−TMD interface regions of Sav1866 and BtuCD.[78,81] The idea that Arg1066 is located near Mg^{2+} in ABP1 is also consistent with the experimental observation that the Arg1066 mutation largely modified the activity of CFTR,[82] likely due to its effect on the binding of ATP to ABP1.

In the X-ray structure of Sav1866, both ICL1 and ICL3 simultaneously contact the two NBDs (NBD1 and NBD2) through the so-called x-loop (sequence is TEVGERG). These interactions are thought to play an important role in stabilizing the NBD−NBD contact in the outward-facing structure.[78] In CFTR, the sequences corresponding to the two x-loops are different from that of Sav1866, and from each other, as follows: IVLGEGG (residues 539−545) in NBD1 and FVLVDGG (residues 1337−1343) in NBD2. In our MD structure in the MgATP-bound state, Lys968 of ICL3 in NBD2 contacts Glu543 of the x-loop in NBD1 (shown in Figure 8E), which is similar to Sav1866. Such an electrostatic interaction, however, was not observed between the x-loop of NBD2 and ICL1 of NBD1. Instead, a part of RI (residues 425−432) in NBD1 was found to contact an upstream portion (residues 1086−1327) of the x-loop in NBD2, which is called the "safety catch"[27] and limits the NBD sliding motion. Therefore, the MD structure around the NBD−TMD interface is, as a whole, similar to that of the outward-facing structure of Sav1866.

Interestingly, as observed from side views of the MD structures (Figure 8A and B), a cavity open to the lateral side of the CFTR protein is present near the NBD−TMD interface in both states. It appears to penetrate the CFTR protein from one side to another, perpendicularly to the vertical pseudo 2-fold axis, and its size appears sufficiently large to allow the passage of a Cl$^-$ ion. It may be hypothesized, then, that the cavity may be a part of the conduction pathway for Cl$^-$ ions from the cytosolic medium. In fact, several Cl$^-$ ions were found in the cavity from the bottom views (Figure 8C and D), despite the fact that there had been no Cl$^-$ ions in the initial structure. This cavity was formed by TM3, 4, 9, and 10, and several arginine and lysine residues (Lys190, Arg242, Lys246, Arg248, Arg352, and Lys978) facing the cavity. It is worth noting that a few Cl$^-$ ions were observed close to the Arg352 residues in both states, which corresponds to the experimental observation that Arg352 significantly contributes to anion conduction in the CFTR channel pore.[41,42] As can be seen from Figure 8C and D, Lys95 of TM1 and Trp1145 of TM12 are located near the vestibule of the pore on the cytoplasmic side. This result is also consistent with those of several combined experimental and computational studies on CFTR.[30,43−47]
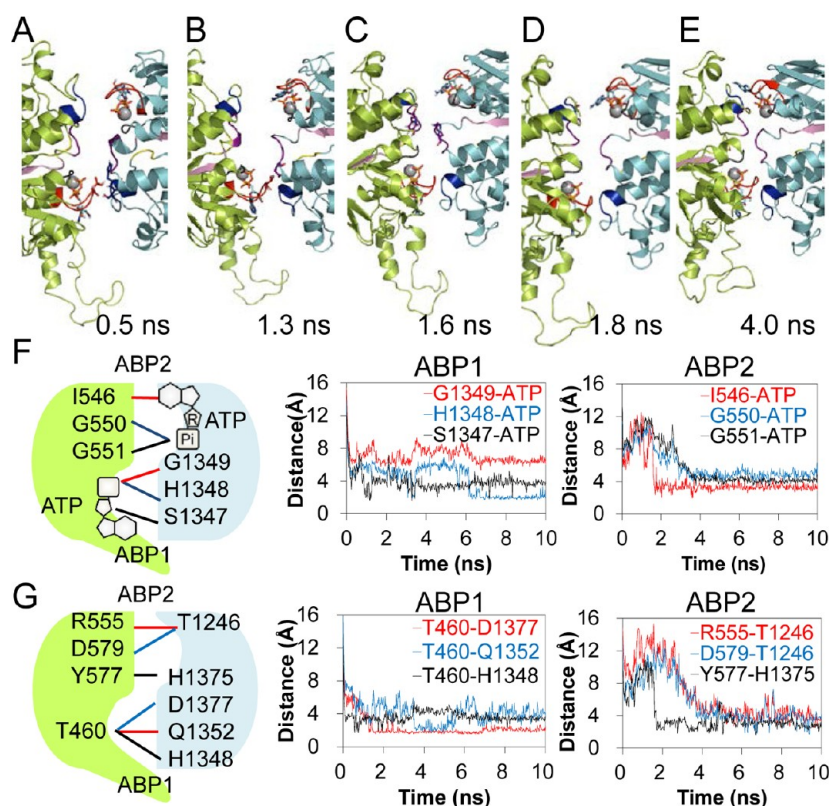
Figure 6. Time course for NBD dimerization. Snapshots of the NBDs at 0.5 (A), 1.3 (B), 1.6 (C), 1.8, (D) and 4.0 ns (E) in the MgATP-bound state. (F) The three ATP-participated interactions found in each ABP (left), time dependence of the minimum distance of each pair in ABP1(center), in ABP2 (right). (G) The three interresidue interactions found in each ABP, time dependence of the minimum distance of each pair in ABP1 (center) and in ABP2 (right).
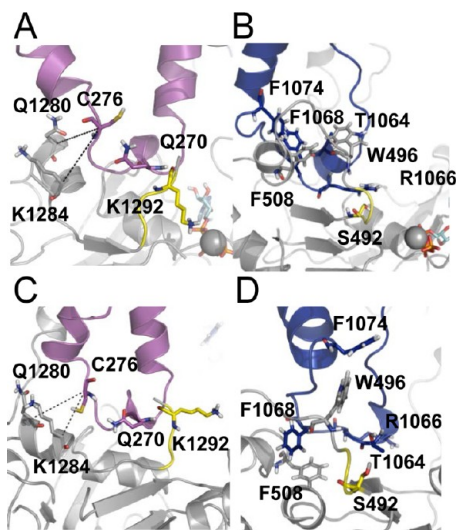

Figure 7. Close-up views around ICL2 and ICL4. (A) ICL2/NBD2 and (B) ICL4/NBD1 in the MgATP-bound state. (C) ICL2/NBD2 and (D) ICL4/NBD1 in the apo state. ICL2, ICL4 and the Q-loop are colored in magenta, blue, and yellow, respectively. Other interacting residues are represented by sticks. There are several interactions between ICL2/NBD2 (C276/Q1280 and C276/K1284) and ICL4/NBD2 (F1068 and F1074/F508, T1064/W496 and R1066/S492).

More interestingly, the internal cavity in the MgATP-bound state is narrower than the cavity that is present in the apo state; however, the cavity size is still large enough to allow preferential movements of the ions along the open channel pore that would be formed in the outward-facing conformation. To examine the closing mechanism of this pore, we measured the TM3-TM9 and TM4-TM10 distances. As a result, for the TM3-TM9 pair, the distance between the residues (Ser185 and Lys190) of TM3 and Lys978 of TM9 was found to be shortened by ∼8−10 Å in both the MgATP-bound and apo states. For the TM4-TM10 pair, in the MgATP-bound state, the Lys1060 of TM10 approached the residues (Val260 and Glu264) of TM4, and hence, their distances were shortened by ∼4−6 Å, whereas in the apo state, the distance was maintained at 13 Å during the simulation. The origin of such distance changes and its concomitant closing of the putative cytoplasmic entrance is likely attributed to the twisting of the TMDs. As observed from a comparison of Figure 8A and B, in the MgATP-bound state, TM9 (cyan) and TM10 (blue) are substantially twisted around the pseudo 2-fold axis such that one can see a part of TM4 (magenta) at the top-left side in Figure 8A, which was initially located on the backside. To explore the origin of these structural changes, we examined the protein dynamics as described below.

Collective Motion of the Protein. The PCA analysis was performed for the last 10 ns of the total 100 ns trajectory to explore global concerted motions generated from thermal fluctuations on the Cα atoms of the protein. The first five PCs correspond to ∼52% of the motion observed in the MgATP-bound simulations and ∼53% of the motion observed in the apo simulations. The contributions of each residue to the PC1 and PC2 are shown in Supporting Information Figure S6. The eigenvectors of PC1 and PC2 in both states were visualized with a porcupine plot, as shown in Figure 9.
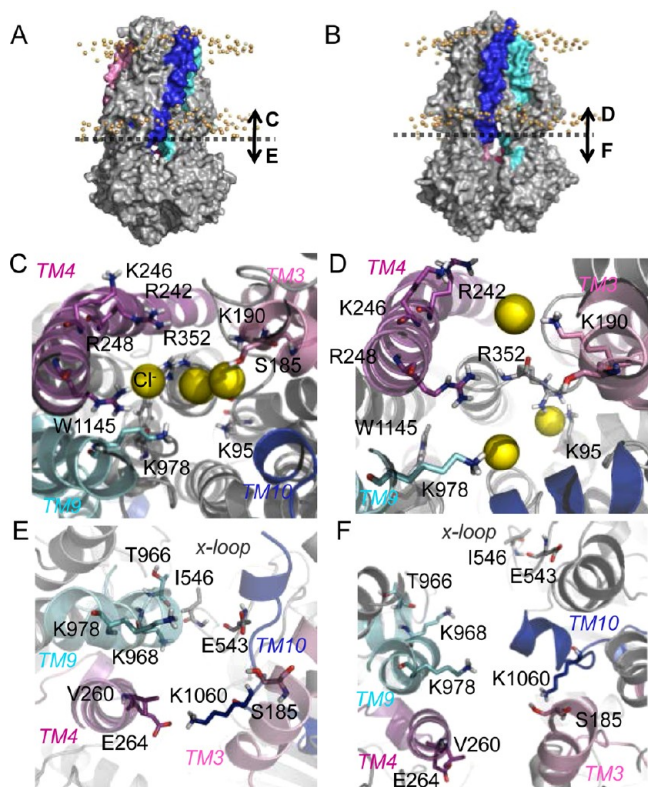
Figure 8. Conformational changes of the internal TM chamber. Overview of the final MD structures in the MgATP-bound (A) and the apo state (B). The TM 3, 4, 9, and 10 are colored in pink, red, cyan, and blue, respectively. The phosphorus atoms of POPC are shown as spheres (orange). Close-up views of the gate entrance in the MgATP-bound state from the bottom (C) and the top (E) and the corresponding views in the apo state from the bottom (D) and the top (F). The Cl⁻ ions and key residues are shown as spheres (yellow) and sticks, respectively.

Figure 9. Principal component analyses for the last 10 ns. The eigenvectors of PC1 and 2 in the MgATP-bound state (A) and in the apo state (B). The direction of movement of each Cα atom is shown with porcupine representation (red), which describes the amplitude of motion with the length of the cone. The proteins are shown in trace (coloring identical to that of Figure 1).

In the apo state, as shown in Figure 9B, both the NBDs have significantly larger amplitudes of fluctuations accompanied by an open−close motion, whereas no appreciable motion is observed in the TMD region. This characteristic was also found in the lower PC modes (see Supporting Information Figure S7). As described previously, the protein in the apo state takes the MsbA "closed-apo"-like conformation in which the two NBDs approach each other with a small degree of contact between their Walker A motifs. As expected, such a structure is dynamically unstable, especially in the NBD region.

In contrast, the PCA in the MgATP-bound state exhibits the presence of a collective motion over a more extended region of the protein. As shown in Figure 9A, both NBDs appear to rotate in the same (clock-wise) direction, and the TMDs also exhibit appreciable amplitudes of fluctuation from the intracellular to extracellular portion. Interestingly, when looking from the extracellular side (top view) in the PC2, the TMDs and NBD-dimer rotate in opposite directions (clockwise and counterclockwise, respectively). Therefore, the NBD dimerization induced by ATP binding could modify the collective motion of the whole protein to significantly activate the motion of the TMD regions. The opposite rotations in the NBD and TMD would lead to a twisted structure of the TMDs, as already shown in Figure 8A, eventually increasing the fluctuation in the extracellular part of the TMDs (shown in Figure 9A). The generation of such 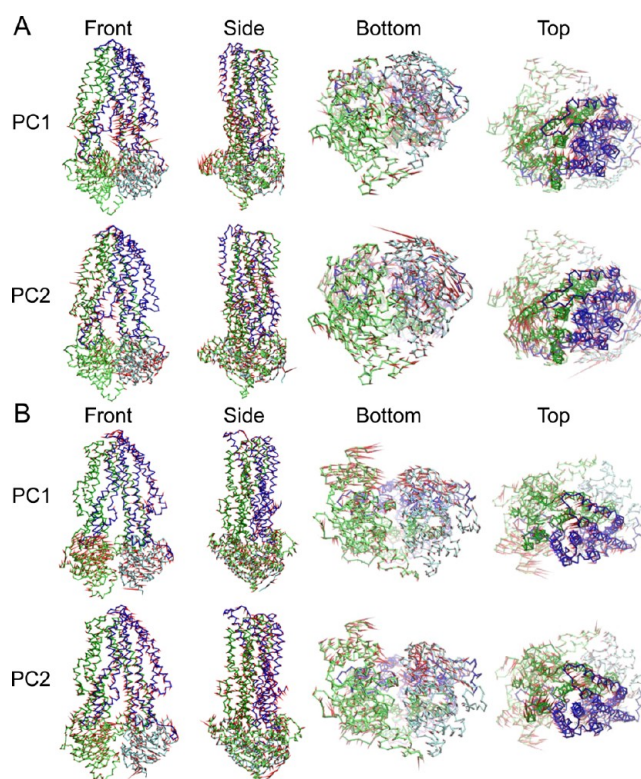motion suggests that the protein structure in the MgATP-bound state is moving to the outward-facing structure; however, more MD simulations of longer duration or other sophisticated simulations are needed to explore a larger conformational change of the protein for direct evidence of this idea.

■ DISCUSSION

Our main goal in this paper was to elucidate the effect of ATP binding on the structure and dynamics of the inward-facing conformation of CFTR. For this purpose, we first performed homology modeling with the "hybrid" template, in which the TMDs were modeled on the basis of the inward-facing conformation of the mouse P-gp transporter, and the NBDs were modeled on the basis of the human CFTR NBD1 and NBD2 structures. In the resulting structure, called "bottom open", the two NBDs were fully separated to be able to catch ATP molecules, and thus, a large cavity was open to the intracellular space (Figure 1). Then, according to the isolated NBD1 crystal structure, two ATP molecules were docked with the NBDs; each of these ATPs was bound to the half-nucleotide binding pocket on the Walker A and Walker B motifs (not on the signature motif) of each NBD. We carried out a 100 ns MD simulation in this MgATP-bound structure and, for comparison, also carried out a similar simulation in the ATP-free (apo) state.

In the MgATP-bound state, the NBD dimerization in a head-to-tail configuration (Figures 3 and 4) took place within 10 ns. To confirm the robustness of this result, we performed three additional simulations. Consequently, the NBD dimerization

always took place within 20 ns (Supporting Information Figure S8A). Such a rapid NBD dimerization might be first driven by the attractive interaction between the adenine ring of ATP and the signature motif in the partner NBD of ABP1 (Figure 5). An in-depth examination of the final MD structure revealed that each of the two ATP molecules was sandwiched between the Walker A and signature motifs, forming many hydrogen bonds (Figure 5) in which the ribose ring and γ-phosphate of the ATPs interact with the residues of the signature motifs in the partner NBDs (Figures 5 and 6). This observation was consistent with experimental results from Zaitseva et al.[83]

In contrast, the NBDs in the apo state failed to form a "canonical" dimer in a head-to-tail fashion and, instead, formed a partial contact structure in which the two NBDs slide along the dimer interface to initiate contact between their Walker A motifs (MsbA "closed-apo"-like conformation).[27,31] We also performed three additional simulations in the apo state. Consequently, the snapshot structure at 20 ns was found to vary from run to run (Supporting InformationFigure S5B). Thus, the MsbA "closed-apo"-like conformation is not necessarily the most stable structure in the apo state. It is likely that in the absence of ATP, the NBDs are in a multiple conformation state, consistent with their large thermal fluctuations (Figure 9).

Taken together, ATP can be referred to as the molecular "glue" that binds the monomers together, as the binding-free energy of ATP was converted to the mechanical work of the NBD dimerization. The present results are consistent with various experimental observations that have shown that ATP binding of the ABC protein is essential for the closure of the NBDs, with the two ATP molecules keeping the NBD heterodimer.[75,83,84]

The mechanism by which the NBDs of ABC transporters power the transport of substrates across cellular membranes still remains unclear. Because the NBDs from different ABC transporters studied so far share a high degree of sequence and structural homology,[85] it seems likely that there is a universal mechanism. There are two hypotheses about the role of ATP as an energy source in the NBD engine as follows: the power stroke is brought about either by ATP binding or by ATP hydrolysis.[86,87] The crystallographic snapshot of MsbA suggested that NBD dimerization and the concomitant structural change in the TMDs from an inward- to an outward-facing conformation take place by binding of AMPPNP (an ATP analogue) to the NBD.[31] The site-directed spin labeling and ESR spectroscopic studies provided results consistent with such crystallographic data and additionally showed that the structure of MsbA trapped by ADP-Vi (posthydrolysis model) was similar to that of the AMPPNP-bound state.[88]

Recently, a similar ESR study was performed for LmrA,[89] an ABC-transporter from *Lactococcus lactis*, and a functional homologue of the essential human multidrug resistance P-gp. In that study, to emulate intermediate catalytic states of the ATP hydrolysis cycle of LmrA, the following states were utilized: (i) the prehydrolysis state emulated by binding of ATP (in the absence of Mg^{2+}) or ADP-BeFx (in the presence of Mg^{2+}) to LmrA; (ii) the transition state by ADP-Vi (Mg^{2+}); (iii) the posthydrolysis state by ADP; and (iv) the apo state. As a result, it was shown that NBD closure and the formation of an outward-facing orientation occurs in the emulated prehydrolysis state. These previous studies might suggest that ATP binding provides the power stroke; however, it remains unclear

whether the nonhydrolyzable analogues of ATP, including ATP in the absence of Mg^{2+}, represent the "nucleotide-bound" state in the real catalytic cycle. In fact, it has been reported that the binding of ATP analogues failed to initiate the channel opening reaction in CFTR.[90,91] The present MD study is the first to describe a role for the natural ligand, ATP and Mg^{2+}, in the ABC transporter superfamily. This work also indicated that the switch from the bottom open to the NBD-dimerized state can be driven only by binding of ATP and Mg^{2+} without the aid of hydrolysis.

The TMDs in our MD structure are still in the inward-facing conformation, which is likely due to insufficient simulation time; however, the results of the PCA indicated that the molecular motion leading to a structural change in the TMDs (twisting motion shown in Figure 9A) had already occurred. In contrast, in the apo state, large dynamic motions of the two NBDs characterized by an open−closed motion were observed, whereas no characteristic motions were found in the TMD regions. It has not been entirely elucidated whether ATP binding to CFTR is essential for channel opening (induced fit) or whether it simply shifts the equilibrium (pre-existing/conformational selection) between states.[90,91] The present MD simulation indicated that the NBD−TMD concerted motion mentioned above was not generated until the NBD dimerization was complete (>30 ns), which may support the former mechanism.

In contrast to ABC transporters bearing only canonical ATP binding pockets, an ATP molecule in CFTR may actually remain bound to the nonconventional binding pocket (ABP1) during the whole gating cycle;[92] consequently, the two NBDs may adopt a "semiopen" (partial dimer) conformation after ATP hydrolysis at the canonical site (ABP2).[10,93] According to our MD results, it is thus expected that a semiopen conformation is formed by retaining contact only at the ABP1 as a result of ATP hydrolysis at ABP2 and the subsequent product release. This model might be supported by the fact that the NBD dimerization occurred asymmetrically with respect to the two ABP sites (Figure 4); interestingly, the formation of ABP1 occurred ahead of that of ABP2. However, Mornon et al.[27] recently proposed a different model for the semiopen state. They constructed the model on the basis of the X-ray structure of MsbA "closed-apo" conformation and located one ATP molecule at a possible contacting point junction between NBD1 and NBD2. More extended and advanced computer simulations and experiments are required to determine which model is reasonable for the semiopen state of CFTR.

■ CONCLUSION

Our MD simulation indicated that the NBDs are first dimerized by binding ATP, which is a power stroke that brings about the concerted motion leading to a significant conformational change of the TMDs. This NBD dimerization took place within only 10 ns. Such a short time scale is an indication of the strong attractive force involved and suggests that the resultant transduced energy may be sufficient to drive the power stroke of the transporter. CFTR is a representative of heterodimeric ABC transporters with one canonical and one noncanonical ABP. Despite such asymmetric nature, in each of the ABPs, an ATP molecule was tightly sandwiched between the Walker A and signature motifs in a canonical fashion. Interestingly, however, the dimerization started from ABP1 (noncanonical pocket) first, followed by ABP2. This trend implies that the NBD−NBD attraction is stronger in ABP1 than in ABP2. An

I

dx.doi.org/10.1021/jp308315w | *J. Phys. Chem. B* XXXX, XXX, XXX−XXX

important finding to be noted here is that several direct interactions between the interfacial residues of the two NBD domains also contribute to the stabilization of the NBD dimer, together with the ATP molecules (Figures 4 and 5), although these interactions alone are not sufficient to drive NBD dimerization based on the results for the apo state. Taken together, our MD results suggest that the free energy gain generated from ATP binding acts as a major driving force for the NBD dimerization and for the occurrence of the subsequent NBD−TMD concerted motions.

■ ASSOCIATED CONTENT

Ⓢ Supporting Information

Figure S1 presents illustrations of the ABPs of CFTR. Figure S2 shows the method for homology modeling, and Figure S3 shows the results from the sequence alignments. Figure S4 presents the comparison of our simulation structures for the apo state with Mornon's model. Figures S5 and S6 present the results of the PCA analyses for the contribution ratio, the plots of the residue positional fluctuations, and the visualizations of the motions of PC3, 4, and 5. This information is available free of charge via the Internet at http://pubs.acs.org.

■ AUTHOR INFORMATION

Corresponding Author
*E-mail: msakurai@bio.titech.ac.jp.
Notes
The authors declare no competing financial interest.

■ ACKNOWLEDGMENTS

■ REFERENCES

(1) Riordan, J. R.; Rommens, J. M.; Kerem, B.; Alon, N.; Rozmahel, R.; Grzelczak, Z.; Zielenski, J.; Lok, S.; Plavsic, N.; Chou, J. L. C.; Drumm, M. L.; Iannuzzi, M. C.; Collins, F. S.; Tsui, L.-C. Science 1989, 245, 1066−1073.
(2) Welsh, M. J.; Smith, A. E. Cell 1993, 73, 1251−1254.
(3) Dean, M.; Allikmets, R. J. Bioenerg. Biomembr. 2001, 33, 475−479.
(4) Higgins, C. F. Res. Microbiol. 2001, 152, 205−210.
(5) Smith, P. C.; Karpowich, N.; Millen, L.; Moody, J. E.; Rosen, J.; Thomas, P. J.; Hunt, J. F. Mol. Cell 2002, 10, 139−149.
(6) Tabcharani, J. A.; Chang, X. B.; Riordan, J. R.; Hanrahan, J. W. Nature 1991, 352, 628−631.
(7) Ostedgaard, L. S.; Baldursson, O.; Welsh, M. J. J. Biol. Chem. 2001, 276, 7689−7692.
(8) Lewis, H. A.; Buchanan, S. G.; Burley, S. K.; Conners, K.; Dickey, M.; Dorwart, M.; Fowler, R.; Gao, X.; Guggino, W. B.; Hendrickson, W. A.; Hunt, J. F.; Kearins, M. C.; Lorimer, D.; Maloney, P. C.; Post, K. W.; Rajashankar, K. R.; Rutter, M. E.; Sauder, J. M.; Shriver, S.; Thibodeau, P. H.; Thomas, P. J.; Zhang, M.; Zhao, X.; Emtage, S. EMBO J. 2004, 23, 282−293.
(9) Mense, M.; Vergani, P.; White, D. M.; Altberg, G.; Nairn, A. C.; Gadsby, D. C. EMBO J. 2006, 25, 4728−4739.
(10) Vergani, P.; Lockless, S. W.; Nairn, A. C.; Gadsby, D. C. Nature 2005, 433, 876−880.
(11) Kerr, I. D. Biochim. Biophys. Acta 2002, 1561, 47−64.
(12) Walker, J. E.; Saraste, M.; Runswick, M. J.; Gay, N. J. EMBO J. 1982, 1, 945−951.
(13) Ambudkar, S. V.; Kim, I. W.; Xia, D.; Sauna, Z. E. FEBS Lett. 2006, 580, 1049−1055.
(14) Schmitt, L.; Benabdelhak, H.; Blight, M. A.; Holland, I. B.; Stubbs, M. T. J. Mol. Biol. 2003, 330, 333−342.
(15) Chen, J.; Lu, G.; Lin, J.; Davidson, A. L.; Quiocho, F. A. Mol. Cell 2003, 12, 651−661.
(16) Schmitt, L.; Tampe, R. Curr. Opin. Struct. Biol. 2002, 12, 754−760.
(17) Hung, L. W.; Wang, I. X.; Nikaido, K.; Liu, P. Q.; Ames, G. F.; Kim, S. H. Nature 1998, 396, 703−707.
(18) Jones, P. M.; George, A. M. J. Phys. Chem. A 2012, 116, 3004−3013.
(19) Hwang, T. C.; Sheppard, D. N. J. Physiol. 2009, 587, 2151−2161.
(20) Riordan, J. R. Annu. Rev. Physiol. 2005, 67, 701−718.
(21) Zhou, Z.; Wang, X.; Liu, H. Y.; Zou, X.; Li, M.; Hwang, T. C. J. Gen. Physiol. 2006, 128, 413−422.
(22) Gadsby, D. C.; Vergani, P.; Csanady, L. Nature 2006, 440, 477−483.
(23) Atwell, S.; Brouillette, C. G.; Conners, K.; Emtage, S.; Gheyi, T.; Guggino, W. B.; Hendle, J.; Hunt, J. F.; Lewis, H. A.; Lu, F.; Protasevich, II; Rodgers, L. A.; Romero, R.; Wasserman, S. R.; Weber, P. C.; Wetmore, D.; Zhang, F. F.; Zhao, X. Protein Eng. Des. Sel. 2010, 23, 375−384.
(24) Lewis, H. A.; Zhao, X.; Wang, C.; Sauder, J. M.; Rooney, I.; Noland, B. W.; Lorimer, D.; Kearins, M. C.; Conners, K.; Condon, B.; Maloney, P. C.; Guggino, W. B.; Hunt, J. F.; Emtage, S. J. Biol. Chem. 2005, 280, 1346−1353.
(25) Aleksandrov, A. A.; Cui, L.; Riordan, J. R. J. Physiol. 2009, 587, 2875−2886.
(26) Mornon, J. P.; Lehn, P.; Callebaut, I. Cell. Mol. Life Sci. 2008, 65, 2594−2612.
(27) Mornon, J. P.; Lehn, P.; Callebaut, I. Cell. Mol. Life Sci. 2009, 66, 3469−3486.
(28) Serohijos, A. W.; Hegedus, T.; Aleksandrov, A. A.; He, L.; Cui, L.; Dokholyan, N. V.; Riordan, J. R. Proc. Natl. Acad. Sci. U.S.A. 2008, 105, 3256−3261.
(29) Norimatsu, Y.; Ivetac, A.; Alexander, C.; Kirkham, J.; O'Donnell, N.; Dawson, D. C.; Sansom, M. S. Biochemistry 2012, 51, 2199−2212.
(30) Dalton, J.; Kalid, O.; Schushan, M.; Ben-Tal, N.; Villa-Freixa, J. J. Chem. Inf. Model. 2012, 52 (7), 1842−1853.
(31) Ward, A.; Reyes, C. L.; Yu, J.; Roth, C. B.; Chang, G. Proc. Natl. Acad. Sci. U.S.A. 2007, 104, 19005−19010.
(32) Altschul, S. F.; Madden, T. L.; Schaffer, A. A.; Zhang, J.; Zhang, Z.; Miller, W.; Lipman, D. J. Nucleic Acids Res. 1997, 25, 3389−3402.
(33) Aller, S. G.; Yu, J.; Ward, A.; Weng, Y.; Chittaboina, S.; Zhuo, R.; Harrell, P. M.; Trinh, Y. T.; Zhang, Q.; Urbatsch, I. L.; Chang, G. Science 2009, 323, 1718−1722.
(34) Thompson, J. D.; Higgins, D. G.; Gibson, T. J. Nucleic Acids Res. 1994, 22, 4673−4680.
(35) Callebaut, I.; Eudes, R.; Mornon, J. P.; Lehn, P. Cell. Mol. Life Sci. 2004, 61, 230−242.
(36) Csanady, L.; Chan, K. W.; Seto-Young, D.; Kopsco, D. C.; Nairn, A. C.; Gadsby, D. C. J. Gen. Physiol. 2000, 116, 477−500.
(37) Marti-Renom, M. A.; Stuart, A. C.; Fiser, A.; Sanchez, R.; Melo, F.; Sali, A. Annu. Rev. Biophys. Biomol. Struct. 2000, 29, 291−325.
(38) Shen, M. Y.; Sali, A. Protein Sci. 2006, 15 (11), 2507−2524.
(39) Melo, F.; Sali, A. Protein Sci. 2007, 16 (11), 2412−2426.
(40) Laskowski, R. A.; Moss, D. S.; Thornton, J. M. J. Mol. Biol. 1993, 231, 1049−1067.
(41) Aubin, C. N.; Linsdell, P. J. Gen. Physiol. 2006, 128, 535−545.
(42) Bai, Y.; Li, M.; Hwang, T. C. J. Gen. Physiol. 2010, 136, 293−309.
(43) Zhou, J. J.; Fatehi, M.; Linsdell, P. J. Membr. Biol. 2007, 216, 123−142.
(44) Wang, W.; El Hiani, Y.; Linsdell, P. J. Gen. Physiol. 2011, 138, 165−178.

(45) Bai, Y.; Li, M.; Hwang, T. C. *J. Gen. Physiol.* **2011**, *138*, 495−507.

(46) Qian, F.; El Hiani, Y.; Linsdell, P. *Pfluegers Arch.* **2011**, *462*, 559−571.

(47) McCarty, N. A. *J. Exp. Biol.* **2000**, *203*, 1947−1962.

(48) Linsdell, P. *Exp. Physiol.* **2006**, *91*, 123−129.

(49) Bai, Y.; Li, M.; Hwang, T. C. *J. Gen. Physiol.* **2010**, *136*, 293−309.

(50) Fatehi, M.; Linsdell, P. *J. Membr. Biol.* **2009**, *228*, 151−164.

(51) Zhou, J.-J.; Li, M.-S.; Qi, J.; Linsdell., P. *J. Gen. Physiol.* **2010**, *135*, 229−245.

(52) Alexander, C.; Ivetac, A.; Liu, X.; Norimatsu, Y.; Serrano, J. R.; Landstrom, A.; Sansom, M.; Dawson, D. C. *Biochemistry* **2009**, *48*, 10078−10088.

(53) Lomize, M. A.; Lomize, A. L.; Pogozheva, I. D.; Mosberg, H. I. *Bioinformatics* **2006**, *22*, 623−625.

(54) Kandt, C.; Ash, W. L.; Tieleman, D. P. *Methods* **2007**, *41*, 475−488.

(55) Nosé, S. *Mol. Phys.* **1984**, *52*, 255−268.

(56) Hoover, W. G. *Phys. Rev. A* **1985**, *31*, 1695−1697.

(57) Parrinello, M.; Rahman, A. *J. Appl. Phys.* **1981**, *52*, 7182−7190.

(58) Hess, B.; Bekker, H.; Berendsen, H. J. C.; Fraaije, J. G. E. M. *J. Comput. Chem.* **1997**, *18*, 1463−1472.

(59) Hess-Coelho, T. A. *J. Mech. Des.* **2007**, *129*, 891−895.

(60) Berendsen, H. J. C.; Postma, J. P. M.; van Gunsteren, W. F.; Hermans, J. *Intermolecular Forces*; Pullman, B., Ed.; Reidel: Dordrecht, 1981; pp 331−342.

(61) Miyamoto, S.; Kollman, P. A. *J. Comput. Chem.* **1992**, *13*, 952−962.

(62) Darden, T.; York, D.; Pedersen, L. *J. Chem. Phys.* **1993**, *98*, 10089−10092.

(63) Essmann, U.; Perera, L.; Berkowitz, M. L.; Darden, T.; Lee, H.; Pedersen, L. G. *J. Chem. Phys.* **1995**, *103*, 8577−8593.

(64) van Der Spoel, D.; Lindahl, E.; Hess, B.; Groenhof, G.; Mark, A. E.; Berendsen, H. J. *J. Comput. Chem.* **2005**, *26*, 1701−1718.

(65) Mark, A. E.; Vanhelden, S. P.; Smith, P. E.; Janssen, L. H. M.; Vangunsteren, W. F. *J. Am. Chem. Soc.* **1994**, *116*, 6293−6302.

(66) van Buuren, A. R.; Marrink, S. J.; Berendsen, H. J. C. *J. Phys. Chem.* **1993**, *97*, 9206−9212.

(67) van Gunsteren, W. F.; Billeter, S. R.; Eising, A. A.; Hünenberger, P. H.; Krüger, P. K.; Mark, A. E.; Scott, W. R. P.; Tironi, I. G. *Biomolecular Simulation: The GROMOS96 Manual and User Guide*; Vdf Hochschulverlag AG an der ETH Zurich: Zurich, Switzerland, 1996.

(68) Berger, O.; Edholm, O.; Jahnig, F. *Biophys. J.* **1997**, *72*, 2002−2013.

(69) Tieleman, D. P.; Berendsen, H. J. *Biophys. J.* **1998**, *74*, 2786−2801.

(70) Lauria, A.; Ippolito, M.; Almerico, A. M. *Comput. Biol. Chem.* **2009**, *33*, 386−390.

(71) Yang, L. W.; Eyal, E.; Bahar, I.; Kitao, A. *Bioinformatics* **2009**, *25*, 606−614.

(72) Humphrey, W.; Dalke, A.; Schulten, K. *J. Mol. Graph.* **1996**, *14*, 33−38.

(73) Chang, X. B.; Hou, Y. X.; Jensen, T. J.; Riordan, J. R. *J. Biol. Chem.* **1994**, *269*, 18572−18575.

(74) Schinkel, A. H.; Kemp, S.; Dolle, M.; Rudenko, G.; Wagenaar, E. *J. Biol. Chem.* **1993**, *268*, 7474−7481.

(75) Newstead, S.; Fowler, P. W.; Bilton, P.; Carpenter, E. P.; Sadler, P. J.; Campopiano, D. J.; Sansom, M. S.; Iwata, S. *Structure* **2009**, *17*, 1213−1222.

(76) Zaitseva, J.; Jenewein, S.; Jumpertz, T.; Holland, I. B.; Schmitt, L. *EMBO J.* **2005**, *24*, 1901−1910.

(77) Csanady, L.; Nairn, A. C.; Gadsby, D. C. *J. Gen. Physiol.* **2006**, *128*, 523−533.

(78) Dawson, R. J.; Locher, K. P. *Nature* **2006**, *443*, 180−185.

(79) Currier, S. J.; Kane, S. E.; Willingham, M. C.; Cardarelli, C. O.; Pastan, I.; Gottesman, M. M. *J. Biol. Chem.* **1992**, *267*, 25153−25159.

(80) Zolnerciks, J. K.; Wooding, C.; Linton, K. J. *FASEB J.* **2007**, *21*, 3937−3948.

(81) Locher, K. P.; Lee, A. T.; Rees, D. C. *Science* **2002**, *296*, 1091−1098.

(82) Cotten, J. F.; Ostedgaard, L. S.; Carson, M. R.; Welsh, M. J. *J. Biol. Chem.* **1996**, *271*, 21279−21284.

(83) Zaitseva, J.; Jenewein, S.; Oswald, C.; Jumpertz, T.; Holland, I. B.; Schmitt, L. *Biochem. Soc. Trans.* **2005**, *33*, 990−995.

(84) Wen, P. C.; Tajkhorshid, E. *Biophys. J.* **2008**, *95*, 5100−5110.

(85) Oswald, C.; Holland, I. B.; Schmitt, L. *Naunyn-Schmiedeberg's Arch. Pharmacol.* **2006**, *372*, 385−399.

(86) Sauna, Z. E.; Ambudkar, S. V. *Mol. Cancer Ther.* **2007**, *6*, 13−23.

(87) Callaghan, R.; Ford, R. C.; Kerr, I. D. *FEBS Lett.* **2006**, *580*, 1056−1063.

(88) Borbat, P. P.; Surendhran, K.; Bortolus, M.; Zou, P.; Freed, J. H.; McHaourab, H. S. *PLoS Biol.* **2007**, *5*, e271.

(89) Hellmich, U. A.; Lyubenova, S.; Kaltenborn, E.; Doshi, R.; van Veen, H. W.; Prisner, T. F.; Glaubitz, C. *J. Am. Chem. Soc.* **2012**, *134*, 5857−5862.

(90) Aleksandrov, A. A.; Chang, X.; Aleksandrov, L.; Riordan, J. R. *J. Physiol.* **2000**, *528* (Pt 2), 259−265.

(91) Wang, W.; Wu, J.; Bernard, K.; Li, G.; Wang, G.; Bevensee, M. O.; Kirk, K. L. *Proc. Natl. Acad. Sci. U.S.A* **2010**, *107*, 3888−3893.

(92) Carson, M. R.; Welsh, M. J. *Am. J. Physiol.* **1993**, *265*, L27−32.

(93) Tsai, M. F.; Li, M.; Hwang, T. C. *J. Gen. Physiol.* **2010**, *135*, 399−414.